THE JOURNAL OF PHYSICAL CHEMISTRY LETTERS
A JOURNAL OF THE AMERICAN CHEMICAL SOCIETY

pubs.acs.org/JPCL

Letter

Coherent Dynamic Nuclear Polarization using Chirped Pulses

Yifan Quan, Manoj V. H. Subramanya, Yifu Ouyang, Michael Mardini, Thierry Dubroca, Stephen Hill, and Robert G. Griffin*

Cite This: *J. Phys. Chem. Lett.* 2023, 14, 4748–4753

Read Online

ACCESS | Metrics & More | Article Recommendations | Supporting Information

ABSTRACT: This paper presents a study of coherent dynamic nuclear polarization (DNP) using frequency swept pulses at 94 GHz which optimize the polarization transfer efficiency. Accordingly, an enhancement $\varepsilon \sim 496$ was observed using 10 mM trityl-OX063 as the polarizing agent in a standard 6:3:1 d_8-glycerol/D_2O/H_2O glassing matrix at 70 K. At present, this is the largest DNP enhancement reported at this microwave frequency and temperature. Furthermore, the frequency swept pulses enhance the nuclear magnetic resonance (NMR) signal and reduce the recycle delay, accelerating the NMR signal acquisition.

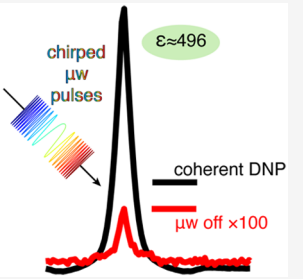

Nuclear magnetic resonance (NMR) is well-known for its high, site-specific resolution and its applicability to a wide variety of chemical, physical, and biological problems. However, it is also known as a low sensitivity technique relative to other forms of spectroscopy. Thus, the development of high frequency dynamic nuclear polarization (DNP) techniques, which offer sensitivity gains of $\sim 10^2$ to 10^3, has enabled many NMR experiments that were otherwise not possible. As a result, DNP has evolved in several guises as the method of choice for enhancing NMR signal intensities in dipole recoupling[1,2] and many other experiments.[3−11]

However, in what are now routine continuous wave (CW) DNP experiments exploiting the solid effect (SE) or cross effect (CE) mechanisms, the signal enhancements, ε, exhibit a frequency dependence proportional to $\sim \omega_{0I}^{-1}$ to $\sim \omega_{0I}^{-2}$, where ω_{0I} is the nuclear Larmor frequency, usually of protons. In the case of the SE, the source of this dependence is the fact that $\varepsilon \sim (\omega_{1S}/\omega_{0I})^2$,[7,12] and ω_{0I} is increasing while ω_{1S}, the electron Rabi field, is constant. In particular, raising ω_{1S} requires unacceptable increases in the CW microwave power applied to the sample. In contrast, coherent or pulsed DNP mechanisms, which manipulate the microwave (μw) frequency, phase, and amplitude, have low duty cycles (~1%) and even substantial pulse power results in low average power. Furthermore, once the pulse power is available, the sequences should behave like INEPT[13] and cross-polarization transfers[14] in NMR, which are field independent. Thus, pulsed experiments can substantially mitigate the field dependence of the enhancement and should provide a promising approach to improve sensitivity in the acquisition of high field NMR spectra.

Accordingly, coherent polarization transfers were initially demonstrated with the nuclear orientation via an electron spin locking (NOVEL) experiment,[15−17] which employs a spin locking sequence on the electrons, and utilizes a Rabi field that matches the lab frame nuclear Larmor frequency, $\omega_{1S} = \omega_{0I}$. A complete theory of NOVEL is published,[15] and it was explored experimentally at 9 and 34 GHz[18,19] where transient oscillations were observed. A ramped version of NOVEL[17] was shown to substantially improve the enhancements. In experiments to date, NOVEL has not shown a frequency dependence and can be considered a "gold standard" for time domain DNP. Nevertheless, the requirement to match the Larmor frequency with the Rabi field renders it a challenging experiment at high fields (>800 MHz for ^{1}H).

A second family of coherent DNP experiments utilizes pulsed μw fields and modulates the Rabi frequency and the pulse timing. In particular, integral multiples of the sum of these two frequencies, $\omega_m = 2\pi/\tau_m$ (the modulation frequency) and ω_{eff} (the effective field), match an integral multiple of ω_{0I} and therefore result in polarization transfer. This approach, TOP-DNP, was first implemented with a train of pulses with constant phase[20,21] and yields an oscillatory nuclear Zeeman polarization frequency profile. More recently, the approach was extended by implementing analogs of the TPPM[22] and XiX[23,24] ^{1}H decoupling sequences and (with much higher power) as BEAM-DNP,[25] all of which seek to "recouple" electrons to ^{1}H.

A third promising approach to coherent DNP methods utilizes relatively low μw power and either magnetic field sweeps or frequency swept (chirped) μw pulses to implement the integrated solid effect (ISE),[26] the stretched solid effect (SSE),[27] and the adiabatic solid effect (ASE).[28] The ISE was

Received: March 17, 2023
Accepted: May 5, 2023
Published: May 15, 2023

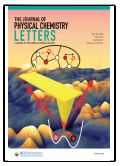

initially performed by adiabatically sweeping the magnetic field through both SE matching conditions,[26,29,30] coherently transferring the electron polarization to the surrounding nuclear spins. It was then shown that ISE can be more readily performed with frequency chirped pulses using an arbitrary waveform generator (AWG) while keeping the magnetic field constant.[27,31] Subsequently, the SSE[27] and ASE[28] were carried out using narrower μw chirped pulses, and it was observed that they can yield larger enhancements than the ISE.

Recently, a theoretical and experimental study was presented that explains many aspects of the spin dynamics associated with the three microwave chirped pulse experiments[32] and provides the impetus for the results presented here. In particular, the ISE utilizes a broad μw frequency sweep through both the forbidden SE double quantum (DQ) and zero quantum (ZQ) matching conditions, e.g., with μw frequency offset chirping from $-\infty$ to ∞ (in practice slightly wider than $\pm\ \omega_{0I}$). In contrast, both the SSE and ASE sweep through only one of the SE matching conditions. The SSE uses a broad sweep terminating at the EPR center, e.g., a sweep from $-\infty$ to 0, while the ASE uses a narrow sweep around one of the SE matching conditions at $\omega_{0S} \pm \omega_{0I}$. To compare the different approaches, we define the polarization transfer ratio E as the gain of the nuclear polarization induced by each DNP pulse, ΔP_I, over the difference between the initial electron and nuclear polarizations, $P_S^0 - P_I^0$. Expressions of the polarization transfer ratios for sweeping over a single SE matching condition, E_{SSE} (for the SSE and ASE), and both matching conditions, E_{ISE} (for the ISE), were derived using the Landau–Zener theory[32] and are

$$E_{SSE} = \frac{\Delta P_I}{P_S^0 - P_I^0} = \frac{2Q}{1+Q} \tag{1}$$

and

$$E_{ISE} = \frac{\Delta P_I}{P_S^0 - P_I^0} = \frac{4}{(1+2Q)(1+Q^{-1})} \tag{2}$$

where

$$Q = 2\pi \frac{\sin^2(\theta_A) M_2}{|\cos(\theta_A)\dot{\omega}|} \tag{3}$$

Here, $\sin(\theta_A) = \omega_{1S}/\omega_{0I}$ and denotes the extent of state mixing, $\dot{\omega}$ is the frequency sweep rate, and M_2 is the second moment of the $|A_{Z+}|$ hyperfine electron–nuclear interaction.

Furthermore, the DNP transfer ratio of an arbitrary frequency chirp over a given EPR line shape can be calculated by integrating over the EPR line using an approach previously developed by our group.[32] The DNP transfer ratios, E_{SSE} and E_{ISE}, denote the *polarization difference* (between electron and nuclear spins) that can be transferred per microwave pulse. As shown in eq 1, the SSE or ASE may reach a DNP transfer ratio greater than 1 when Q is also greater than 1, approaching $E = 2$ for $Q \gg 1$. A large Q value is achieved by applying a strong μw pulse, making ω_{1S}/ω_{0I} large, combined with a slow frequency chirp (small $\dot{\omega}$).

In an ideal swept frequency experiment, the electron polarization goes from +1 to −1 after a single μw pulse; thus, the polarization transfer ratio is $E = 2$, and the surrounding N nuclear spins each gain a polarization of E/N. Furthermore, the nuclear polarization *cannot* be enhanced more than the electron polarization as it is the polarization *difference* that is transferred and oscillating. When the nuclear polarization is larger than the electron polarization, the nuclei will lose polarization to the electron. This reversal of polarization transfer is also why the ISE exhibits lower enhancement than the SSE in this regime. Theory demonstrates that the ISE has a maximum transfer ratio of 0.686, lower than 2 for the SSE, understood by realizing that a sweep through the first SE matching condition, when the DNP process is efficient, yields an electron polarization that is inverted; experimental verification of this prediction via EPR experiments is provided in the Supporting Information. Therefore, when transitioning through the subsequent matching condition, the polarization is transferred from the nuclear spins back to the electron spin or equivalently the nuclear spins are polarized toward the other direction compared to the first matching condition. This limits the efficiency of the ISE. A link to a video illustrating the electron and nuclear spin polarizations is provided in the Supporting Information. The trajectory of the electron spin polarization vector is simulated using the SpinEvolution software[33] with one electron spin hyperfine coupled to five nuclear spins.

In summary, it appears that a DNP transfer ratio E_{SSE} of 2 obtained with the ASE and SSE is, thus far, the more efficient pulsed technique. This transfer ratio compares to a value of 0.686 for the ISE,[20] which is derived from eq 2, and 1.3 for NOVEL.[10] TOP-, XiX-, and TPPM-DNP can have a similar theoretical maximum transfer ratio as NOVEL per pulse train. However, TOP-DNP[20] and XiX-DNP[24] require longer irradiation periods, which yields additional decoherence of the spins, and therefore an efficiency lower than NOVEL. The high DNP transfer ratio of chirped pulses is attributable to the adiabatic level crossing that is intrinsically more efficient than other transition pumping pulsed techniques. This is also the case for ramped-amplitude NOVEL[17] and BEAM-DNP.[25] These estimates are discussed in more detail in the Supporting Information. Finally, chirped DNP allows utilization of all of the electron spins by integrating the EPR frequencies, which is an advantage over single frequency pulsed techniques. Similar improvements have been demonstrated for other frequency modulation DNP schemes.[34−37]

To date, most pulsed DNP experiments have been performed at X-band and Q-band[17−20,24,25] because of the availability of pulsed microwave amplifiers at these frequencies. The single time domain DNP experiment performed at W-band (3.4 T) is the SSE/ISE experiment mentioned previously[27] using the HiPER (High Power quasi-optical EPR) spectrometer, a design first developed by Smith et al.[38,39] The spectrometer used then was equipped with a 94 GHz, 1 kW extended interaction klystron (EIK) and NMR console and achieved an enhancement $\varepsilon \sim 70$.

In this work, we use an upgraded version of the National High Magnetic Field Laboratory (NHMFL) HiPER instrument.[39] In addition, the improved understanding of the spin dynamics of chirped pulsed DNP permits an optimization of the DNP efficiency, leading to an enhancement of $\varepsilon \sim 496$ with ∼250–300 W of microwave power. This is a significant improvement in the efficiency of the DNP process, even with only about 1/4 of the μw power available in the previously reported experiment. The lower μw power is due to the limited AWG output power and aging of the EIK.

METHODS

Three trityl-OX063 samples—(1) 10 mM trityl in the 6:3:1 glycerol-d_8/D_2O/H_2O glassing matrix, (2) 20 mM trityl in

https://doi.org/10.1021/acs.jpclett.3c00726
J. Phys. Chem. Lett. 2023, 14, 4748−4753

6:3:1 d_8-glycerol/D_2O/H_2O, and (3) 10 mM trityl in 6:4 d_8-glycerol/H_2O—were prepared for the DNP experiments. All of the samples were thoroughly degassed by storing the matrix material inside fluorinated ethylene propylene (FEP) vials in an argon atmosphere inside a glovebox for more than a week. During the storage period, FEP allows oxygen molecules to diffuse out of the solutions through the FEP tubes, while remaining impermeable to liquids such as glycerol and water. In addition, the samples were transferred inside FEP tubes (3 mm OD, 2 mm ID, 30 mm long, ~70 μL volume) and sealed by welding the tube to itself inside of the glovebox in order to minimize oxygen contamination. The long nuclear T_{1n} at 70 K reported below confirms that the samples were well degassed.

The DNP experiments were performed with the recently upgraded NHMFL HiPER spectrometer,[38,39] and the upgrade consists of the addition of a Keysight M9502A AWG,[40] SpecMan4EPR 3.0 for the control software,[41] and a custom designed NMR system. The NMR instrument is composed of a single channel RF coil, with external tuning and matching circuits following a previously established design[27] and powered by a Direct Drive Agilent NMR console (10−245 MHz, 250 W). Finally, the magnet is fitted with a helium flow cryostat allowing low temperature measurement compatible with the radio frequency detection system.

As discussed above, a large ω_{1S} and low $\dot{\omega}$, to maximize Q, are preferred to optimize the efficiency of chirped DNP. Therefore, 12 μs pulses (the maximum allowed by the EIK) were used for all experiments in order to minimize $\dot{\omega}$. In addition, to increase the DNP enhancement, we set the magnetic field to match the SE condition at 93.7 GHz frequency where the EIK produces the optimal power (~250 W, $\omega_{1S}/2\pi \sim 20$ MHz, see Figure 1). A train of NMR saturating pulses was applied to dephase the nuclear spin polarization prior to each DNP buildup, and a solid echo ^{1}H experiment was used to monitor the DNP enhanced NMR signal.

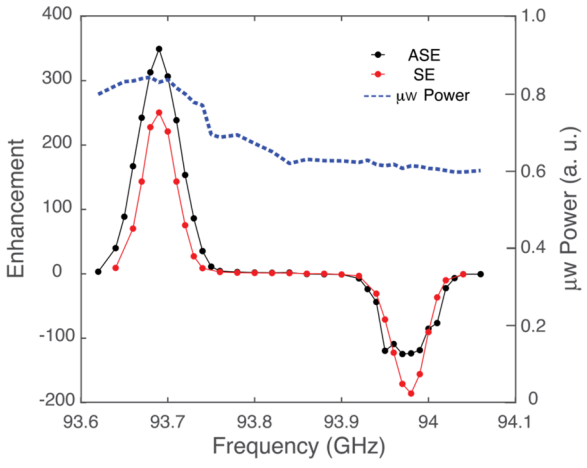

Figure 1. Field profile of the DNP enhancement comparing ASE and SE for sample 1, 10 mM trityl-OX063 in 6:3:1 d_8-glycerol/D_2O/H_2O. The DNP enhanced NMR signals were measured after 150 s of DNP using 12 μs microwave pulses with a repetition delay of 1.2 ms. For the ASE experiment, a 40 MHz frequency chirp was applied, while for the SE no chirping was employed. The dashed line shows the frequency dependence of the microwave power profile (arbitrary units) produced by the EIK and at 93.7 GHz is ~250 W.

Shown in Figure 1 is the DNP Zeeman field profile recorded for 10 mM trityl-OX063 at 70 K using the ASE under optimized conditions. The enhancements were recorded using a 12 μs, 40 MHz frequency chirp with a repetition delay of 1.2 ms. For the data in Figure 1, the chirps were performed for a total of 150 s. These results are compared to the SE Zeeman field profile recorded without chirping. In addition, the relative microwave power profile of the EIK is included in the figure as the dashed line. The echo detected EPR spectrum is shown in the Supporting Information. The ZQ SE/ASE enhancement at 93.98 GHz is significantly smaller than the DQ enhancement due to the lower ω_{1S} at a high frequency.

The ASE results in larger enhancements for the DQ transition, while the SE appears more efficient than the ASE for the ZQ transition due to the lower microwave power. This observation brings to focus several experimental aspects of the ASE. Given a fixed pulse length, one can increase the sweep width to bring more electron spins across the matching condition. However, since this increases the sweep rate $\dot{\omega}$, the DNP transfer ratio decreases (see eqs 1 and 3 and Figure 2 in ref 32). This decrease of the DNP transfer ratio can be compensated by increasing ω_{1S} to keep Q large. At sufficiently high ω_{1S}, the broader sweep can be applied to cover additional electron spins, eventually transitioning to SSE. In the other extreme, where the microwave ω_{1S} is lower, then the SE without chirping can be more efficient than ASE with chirping, which we observe for the ZQ transition. The optimization of the sweep width for the sample at 70 K is shown in Figure 2.

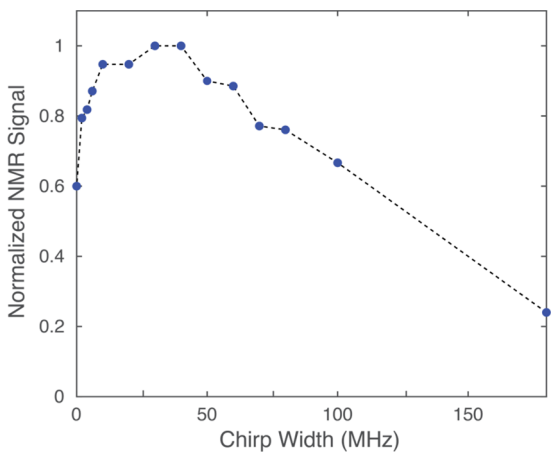

Figure 2. Normalized NMR signal intensity of sample 1, 10 mM trityl-OX063 in 6:3:1 d_8-glycerol/D_2O/H_2O, enhanced by ASE with different chirp widths. All of the sequences were with the same 12 μs pulse length. With no chirping, the left most point is the SE, while the right most point becomes the SSE with 180 MHz of chirping.

The first point is without chirping and corresponds to the SE, while the last point uses a chirp width of 180 MHz and corresponds to the SSE. Additionally, the optimum repetition delay was determined to be 1.2 ms, which depends on the pulse sequence, the T_{1e}, and the DNP transfer ratio.

Following optimization, the DNP buildup for the ASE is compared to the NMR saturation recovery, shown in Figure 3. The rise time of the optimized ASE is estimated to be $T_{rise} \approx 250$ s, significantly shorter than $T_{1n} \approx 460$ s. Figure 4 shows the comparison of the DNP enhanced solid echo signal with the optimized 40 MHz frequency swept ASE pulses (see Figure 2) and the thermal signal (scaled by 100, taken overnight with

https://doi.org/10.1021/acs.jpclett.3c00726
J. Phys. Chem. Lett. 2023, 14, 4748−4753

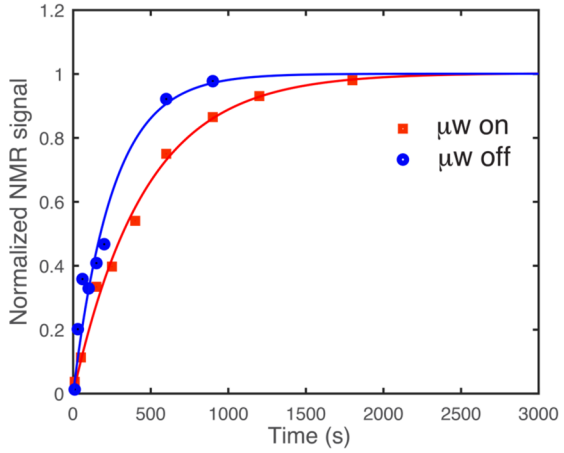

Figure 3. Saturation recovery curves of sample 1, 10 mM trityl-OX063 in 6:3:1 glycerol-d_8/D_2O/H_2O, at 70 K with the microwave on (T_{rise} ~ 250 s for the DNP rise time with ASE) and off (T_{1n} ~ 460 s). They are both normalized for comparison.

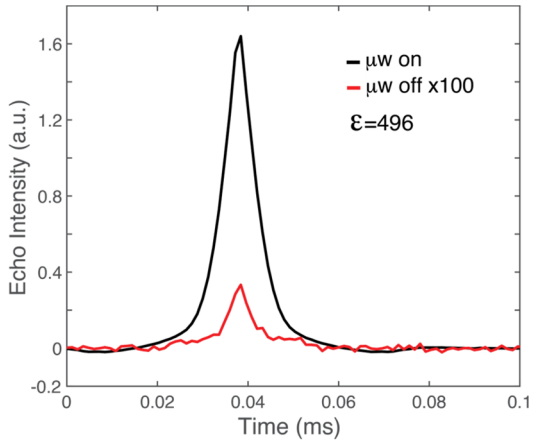

Figure 4. ^{1}H solid echo signal of sample 1, 10 mM trityl-OX063 in 6:3:1 d_8-glycerol/D_2O/H_2O, at 70 K with optimized ASE (40 MHz chirp pulses) compared to the thermal NMR signal. A higher input power to the EIK is used for this measurement, giving an output power of ~300 W. The thermal signal was measured with 1800 s recovery time (~4T_{1n}) and scaled by a factor 100 in the plot for comparison. The enhancement is calculated to be ε ~ 496.

a recovery time of 1800s ~ 4 × T_{1n}). A slightly higher power (~300 W) was made available from the EIK by manually overriding the control software for this experiment, resulting in an enhancement of ε ~ 496. The error in the measurement is estimated to be 5%, mainly from uncertainty in the thermal signal. As the DNP rise time is much faster than the nuclear spin−lattice relaxation, the NMR signal for microwave $\varepsilon_{on}/\varepsilon_{off}$ can be even larger when the nuclear spin polarization is not yet fully recovered, e.g., S_{on}/S_{off} > 1000 at the same 150 s time of DNP build-up and nuclear spin polarization recovery. In this case, DNP not only enhances the NMR signal but also reduces the repetition delay allowing faster NMR acquisition and an even larger increase of the signal-to-noise per unit time than the enhancement alone implies.

In addition, we compared the enhancements obtained from the SE, ASE, SSE, and ISE at 70 K with the same ω_{1S} (with an EIK output of ~250 W instead of ~300 W used in Figure 4), and these results are tabulated in Table 1. The ASE is the most efficient pulse sequence at this relatively modest ω_{1S}, as Figure 2 suggests. Theoretically, when the microwave power is sufficient, the SSE that covers more electron spins should be more efficient than ASE. In practice, however, since the ASE uses a narrower and thus slower frequency chirp than the SSE, it achieves a higher Q with the same ω_{1S} and becomes the more efficient approach for our conditions. Furthermore, the enhancement of the 10 mM sample was quickly measured at 90 and 110 K without a full reoptimization, and an enhancement above 300 was obtained at these temperatures.

Table 1. Comparison of the DNP Enhancements of the Sample 1, 10 mM Trityl-OX063 in 6:3:1 Glycerol-d_8/D_2O/H_2O, at 70 K with Difference Chirped Pulse Techniques

pulse	chirp width	ε
SE	0 MHz	272
ASE	40 MHz	480
SSE	180 MHz	192
ISE	360 MHz	28

Table 2 summarizes the DNP enhancements with optimized ASE for each of the three samples at 70 K. The 10 mM sample 1 shows a much higher enhancement than the 20 mM sample 2. Although the fully protonated sample 3 has a low enhancement, it has 4 times more protons, so we estimate comparable overall polarization transfer to that of sample 1. Furthermore, we performed a temperature dependent study on sample 2, which has a reasonable nuclear T_{1n} to fit into the instrumental time available. This is plotted in Figure 5. A significant decrease of the enhancement is observed from 110 to 130 K. A similar effect was observed previously for BDPA in oTP, although at 240 K.[42]

Table 2. DNP Enhancement of the Samples with Optimized ASE As Well As the T_{1n} at 70 K

sample	Trityl-OX063	glycerol-d_8/D_2O/H_2O	T_{1n}	ε
1	10 mM	6:3:1	460 s	496
2	20 mM	6:3:1	96 s	255
3	10 mM	6:0:4	54 s	125

In summary, we studied coherent DNP with chirped pulses at 94 GHz using the HiPER instrument. In particular, we

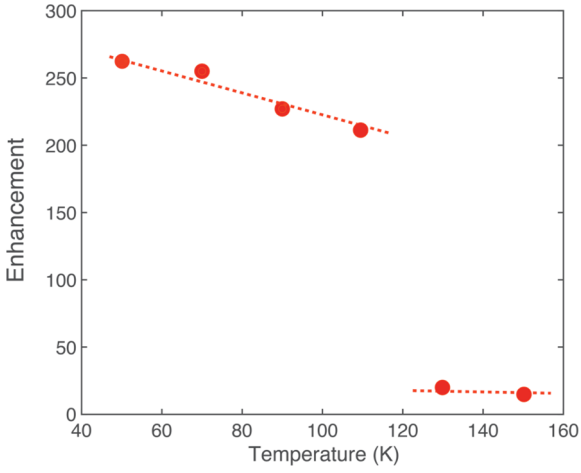

Figure 5. Temperature dependence of the DNP enhancement of the optimized ASE for sample 2, 20 mM trityl-OX063 in 6:3:1 d_8-glycerol/D_2O/H_2O.

https://doi.org/10.1021/acs.jpclett.3c00726
J. Phys. Chem. Lett. 2023, 14, 4748−4753

studied three trityl-OX063 samples in the d_8-glycerol/D_2O/H_2O mixture glassing matrix, a typical matrix for MAS NMR. An enhancement of $\varepsilon \sim 496$, approaching the theoretical maximum of 658, was measured for sample 1, 10 mM trityl-OX063 in 6:3:1 d_8-glycerol/D_2O/H_2O at 70 K with the ASE pulse sequence. Compared to the previous pulsed experiment at 94 GHz using chirped pulses,[27] a significant improvement was achieved, due to a better understanding of the spin dynamics.[32] To our knowledge, this is also a record enhancement achieved at this magnetic field and temperature for such a sample. With the capability of manipulating the μw frequency, phase, and amplitude, a high enhancement can be achieved using pulsed DNP techniques. Furthermore, we have shown that it is critical to understand the spin physics, which can lead to advances in the DNP techniques and applications.

We have also compared different chirped DNP pulse sequences. In practice, with limited microwave power and duty cycle, the ASE, which is less technically demanding, can be the more efficient DNP approach compared to the SE, SSE, and ISE. In addition, not only can DNP enhance the NMR signal but it can also reduce the NMR repetition delay, accelerating acquisition. Finally, we observe that the DNP enhancement remains high below 110 K but drops considerably above 130 K for glycerol−D_2O−H_2O mixtures.

As mentioned above, pulsed DNP is still in its infancy and is mostly limited to experiments at the X-band and Q-band. However, in experiments reported here at 94 GHz, we achieved $\varepsilon = 496$, which is presently a record enhancement for this frequency and temperature. Thus, we believe that our experimental results at the W-band are compelling evidence that coherent DNP methods are extremely promising approaches for spectroscopy at higher fields, where the resolution of NMR spectra is optimized. Accordingly, it is important to develop the instrumentation and expertise to explore and develop these methods further.

■ ASSOCIATED CONTENT

Supporting Information

The Supporting Information is available free of charge at https://pubs.acs.org/doi/10.1021/acs.jpclett.3c00726.

DNP transfer ratios, W-band EPR, study of electron coherence after SSE, movie demonstrating the electron and nuclear polarizations during ISE (PDF)

■ AUTHOR INFORMATION

Corresponding Author

Robert G. Griffin − *Francis Bitter Magnet Laboratory and Department of Chemistry, Massachusetts Institute of Technology, Cambridge, Massachusetts 02139, United States;* orcid.org/0000-0003-1589-832X; Email: rgg@mit.edu

Authors

Yifan Quan − *Francis Bitter Magnet Laboratory and Department of Chemistry, Massachusetts Institute of Technology, Cambridge, Massachusetts 02139, United States*

Manoj V. H. Subramanya − *National High Magnetic Field Laboratory, Tallahassee, Florida 32310, United States; Department of Physics, Florida State University, Tallahassee, Florida 32310, United States*

Yifu Ouyang − *Francis Bitter Magnet Laboratory and Department of Chemistry, Massachusetts Institute of Technology, Cambridge, Massachusetts 02139, United States*

Michael Mardini − *Francis Bitter Magnet Laboratory and Department of Chemistry, Massachusetts Institute of Technology, Cambridge, Massachusetts 02139, United States*

Thierry Dubroca − *National High Magnetic Field Laboratory, Tallahassee, Florida 32310, United States*

Stephen Hill − *National High Magnetic Field Laboratory, Tallahassee, Florida 32310, United States; Department of Physics, Florida State University, Tallahassee, Florida 32310, United States;* orcid.org/0000-0001-6742-3620

Complete contact information is available at: https://pubs.acs.org/10.1021/acs.jpclett.3c00726

Notes

The authors declare no competing financial interest.

■ ACKNOWLEDGMENTS

This work was supported by the National Institutes of Health through grants (GM132997 and AG058504) to R.G.G., by the Swiss National Science Foundation through a grant (P500PN_202639) to Y.Q., and by the U.S. Department of Energy under Award DE-SC0020260 to S.H. The experiments were performed at the National High Magnetic Field Laboratory (NHMFL) funded by the National Science Foundation Division of Materials Research (DMR-1644779 and DMR-2128556) and the State of Florida.

■ REFERENCES

(1) Bennett, A. E.; Griffin, R. G.; Vega, S. Recoupling of Homo- and Heteronuclear Dipolar Interactions in Rotating Solids. *NMR Basic Principles and Progress* **1994**, *33*, 1−77.

(2) Griffiths, J. M.; Griffin, R. G. Nuclear-Magnetic-Resonance Methods for Measuring Dipolar Couplings in Rotating Solids. *Anal. Chim. Acta* **1993**, *283*, 1081−1101.

(3) Becerra, L. R.; Gerfen, G. J.; Temkin, R. J.; Singel, D. J.; Griffin, R. G. Dynamic Nuclear Polarization with a Cyclotron Resonance Maser at 5 T. *Phys. Rev. Lett.* **1993**, *71*, 3561−3564.

(4) Maly, T.; Debelouchina, G. T.; Bajaj, V. S.; Hu, K. N.; Joo, C. G.; Mak-Jurkauskas, M. L.; Sirigiri, J. R.; van der Wel, P. C.; Herzfeld, J.; Temkin, R. J.; Griffin, R. G. Dynamic Nuclear Polarization at High Magnetic Fields. *J. Chem. Phys.* **2008**, *128*, 052211.

(5) Barnes, A. B.; De Paepe, G.; van der Wel, P. C.; Hu, K. N.; Joo, C. G.; Bajaj, V. S.; Mak-Jurkauskas, M. L.; Sirigiri, J. R.; Herzfeld, J.; Temkin, R. J.; Griffin, R. G. High-Field Dynamic Nuclear Polarization for Solid and Solution Biological Nmr. *Appl. Magn. Reson.* **2008**, *34*, 237−263.

(6) Ni, Q. Z.; Daviso, E.; Can, T. V.; Markhasin, E.; Jawla, S. K.; Swager, T. M.; Temkin, R. J.; Herzfeld, J.; Griffin, R. G. High Frequency Dynamic Nuclear Polarization. *Acc. Chem. Res.* **2013**, *46*, 1933−1941.

(7) Lilly Thankamony, A. S.; Wittmann, J. J.; Kaushik, M.; Corzilius, B. Dynamic Nuclear Polarization for Sensitivity Enhancement in Modern Solid-State Nmr. *Prog. Nucl. Magn. Reson. Spectrosc.* **2017**, *102*, 120−195.

(8) Jaudzems, K.; Polenova, T.; Pintacuda, G.; Oschkinat, H.; Lesage, A. Dnp Nmr of Biomolecular Assemblies. *J. Struct Biol.* **2019**, *206*, 90−98.

(9) Griffin, R. G.; Swager, T. M.; Temkin, R. J. High Frequency Dynamic Nuclear Polarization: New Directions for the 21st Century. *J. Magn. Reson.* **2019**, *306*, 128−133.

(10) Plainchont, B.; Berruyer, P.; Dumez, J. N.; Jannin, S.; Giraudeau, P. Dynamic Nuclear Polarization Opens New Perspectives

for Nmr Spectroscopy in Analytical Chemistry. *Anal. Chem.* **2018**, *90*, 3639−3650.
(11) Biedenbander, T.; Aladin, V.; Saeidpour, S.; Corzilius, B. Y Dynamic Nuclear Polarization for Sensitivity Enhancement in Biomolecular Solid-State Nmr. *Chem. Rev.* **2022**, *122*, 9738−9794.
(12) Smith, A. A.; Corzilius, B.; Barnes, A. B.; Maly, T.; Griffin, R. G. Solid Effect Dynamic Nuclear Polarization and Polarization Pathways. *J. Chem. Phys.* **2012**, *136*, 015101.
(13) Bax, A.; Freeman, R.; Kempsell, S. P. Natural Abundance 13c-13c Coupling Observed Via Double-Quantum Coherence. *J. Am. Chem. Soc.* **1980**, *102*, 4849−4851.
(14) Pines, A.; Gibby, M. G.; Waugh, J. S. Proton-Enhanced Nmr of Dilute Spins in Solids. *J. Chem. Phys.* **1973**, *59*, 569−590.
(15) Henstra, A.; Wenckebach, W. T. The Theory of Nuclear Orientation Via Electron Spin Locking (Novel). *Mol. Phys.* **2008**, *106*, 859−871.
(16) Can, T. V.; Ni, Q. Z.; Griffin, R. G. Mechanisms of Dynamic Nuclear Polarization in Insulating Solids. *J. Magn. Reson.* **2015**, *253*, 23−35.
(17) Can, T. V.; Weber, R. T.; Walish, J. J.; Swager, T. M.; Griffin, R. G. Ramped-Amplitude Novel. *J. Chem. Phys.* **2017**, *146*, 154204.
(18) Can, T. V.; Walish, J. J.; Swager, T. M.; Griffin, R. G. Time Domain Dnp with the Novel Sequence. *J. Chem. Phys.* **2015**, *143*, 054201.
(19) Can, T. V.; Tan, K. O.; Yang, C.; Weber, R. T.; Griffin, R. G. Time Domain Dnp at 1.2 T. *J. Magn. Reson.* **2021**, *329*, 107012.
(20) Tan, K. O.; Yang, C.; Weber, R. T.; Mathies, G.; Griffin, R. G. Time-Optimized Pulsed Dynamic Nuclear Polarization. *Sci. Adv.* **2019**, *5*, eaav6909.
(21) Tan, K. O.; Jawla, S.; Temkin, R. J.; Griffin, R. G. Pulsed Dynamic Nuclear Polarization. *eMagRes* **2019**, *8*, 339−351.
(22) Bennett, A. E.; Rienstra, C. M.; Auger, M.; Lakshmi, K. V.; Griffin, R. G. Heteronuclear Decoupling in Rotating Solids. *J. Chem. Phys.* **1995**, *103*, 6951−6958.
(23) Detken, A.; Hardy, E. H.; Ernst, M.; Meier, B. H. Simple and Efficient Decoupling in Magic-Angle Spinning Solid-State Nmr: The Xix Scheme. *Chem. Phys. Lett.* **2002**, *356*, 298−304.
(24) Redrouthu, V. S.; Mathies, G. Efficient Pulsed Dynamic Nuclear Polarization with the X-Inverse-X Sequence. *J. Am. Chem. Soc.* **2022**, *144*, 1513−1516.
(25) Wili, N.; Nielsen, A. B.; Voelker, L. A.; Schreder, L.; Nielsen, N. C.; Jeschke, G.; Tan, K. O. Designing Broadband Pulsed Dynamic Nuclear Polarization Sequences in Static Solids. *Sci. Adv.* **2022**, *8*, DOI: 10.1126/sciadv.abq0536.
(26) Henstra, A.; Wenckebach, W. T. Dynamic Nuclear Polarisation Via the Integrated Solid Effect I: Theory. *Mol. Phys.* **2014**, *112*, 1761−1772.
(27) Can, T. V.; McKay, J. E.; Weber, R. T.; Yang, C.; Dubroca, T.; van Tol, J.; Hill, S.; Griffin, R. G. Frequency-Swept Integrated and Stretched Solid Effect Dynamic Nuclear Polarization. *J. Phys. Chem. Lett.* **2018**, *9*, 3187−3192.
(28) Tan, K. O.; Weber, R. T.; Can, T. V.; Griffin, R. G. Adiabatic Solid Effect. *J. Phys. Chem. Lett.* **2020**, *11*, 3416−3421.
(29) Henstra, A.; Dirksen, P.; Wenckebach, W. T. Enhanced Dynamic Nuclear Polarization by the Integrated Solid Effect. *Phys. Lett.* **1988**, *A134*, 134.
(30) Eichhorn, T. R.; van den Brandt, B.; Hautle, P.; Henstra, A.; Wenckebach, W. T. Dynamic Nuclear Polarisation Via the Integrated Solid Effect Ii: Experiments on Naphthalene-H(8) Doped with Pentacene-D(14). *Mol. Phys.* **2014**, *112*, 1773−1782.
(31) Can, T. V.; Weber, R. T.; Walish, J. J.; Swager, T. M.; Griffin, R. G. Frequency-Swept Integrated Solid Effect. *Angew. Chem., Int. Ed. Engl.* **2017**, *56*, 6744−6748.
(32) Quan, Y. F.; Steiner, J.; Ouyang, Y. F.; Tan, K. O.; Wenckebach, W. T.; Hautle, P.; Griffin, R. G. Integrated, Stretched, and Adiabatic Solid Effects. *J. Phys. Chem. Lett.* **2022**, *13*, 5751−5757.
(33) Veshtort, M.; Griffin, R. G. Spinevolution: A Powerful Tool for the Simulation of Solid and Liquid State Nmr Experiments. *J. Magn. Reson.* **2006**, *178*, 248−282.
(34) Hovav, Y.; Feintuch, A.; Vega, S.; Goldfarb, D. Dynamic Nuclear Polarization Using Frequency Modulation at 3.34t. *J. Magn. Reson.* **2014**, *238*, 94−105.
(35) Judge, P. T.; Sesti, E. L.; Alaniva, N.; Saliba, E. P.; Price, L. E.; Gao, C.; Halbritter, T.; Sigurdsson, S. T.; Kyei, G. B.; Barnes, A. B. Characterization of Frequency-Chirped Dynamic Nuclear Polarization in Rotating Solids. *J. Magn. Reson.* **2020**, *313*, 106702.
(36) Ajoy, A.; Nazaryan, R.; Liu, K.; Lv, X.; Safvati, B.; Wang, G.; Druga, E.; Reimer, J. A.; Suter, D.; Ramanathan, C.; Meriles, C. A.; Pines, A. Enhanced Dynamic Nuclear Polarization Via Swept Microwave Frequency Combs. *Proc. Natl. Acad. Sci. U. S. A.* **2018**, *115*, 10576−10581.
(37) Zangara, P. R.; Dhomkar, S.; Ajoy, A.; Liu, K.; Nazaryan, R.; Pagliero, D.; Suter, D.; Reimer, J. A.; Pines, A.; Meriles, C. A. Dynamics of Frequency-Swept Nuclear Spin Optical Pumping in Powdered Diamond at Low Magnetic Fields. *Proc. Natl. Acad. Sci. U. S. A.* **2019**, *116*, 2512−2520.
(38) Cruickshank, P. A. S.; Bolton, D. R.; Robertson, D. A.; Hunter, R. I.; Wylde, R. J.; Smith, G. M. A Kilowatt Pulsed 94 Ghz Electron Paramagnetic Resonance Spectrometer with High Concentration Sensitivity, High Instantaneous Bandwidth, and Low Dead Time. *Rev. Sci. Instrum.* **2009**, *80*, 103102.
(39) Hunter, R. I.; Cruickshank, P. A. S.; Bolton, D. R.; Riedi, P. C.; Smith, G. M. High Power Pulsed Dynamic Nuclear Polarisation at 94 Ghz. *Phys. Chem. Chem. Phys.* **2010**, *12*, 5752−5756.
(40) Subramanya, M. V. H.; Marbey, J.; Kundu, K.; McKay, J. E.; Hill, S. Broadband Fourier-Transform-Detected Epr at W-Band. *Appl. Magn. Reson.* **2023**, *54*, 165−181.
(41) Epel, B.; Gromov, I.; Stoll, S.; Schweiger, A.; Goldfarb, D. Spectrometer Manager: A Versatile Control Software for Pulse Epr Spectrometers. *Concepts in Magnetic Resonance Part B-Magnetic Resonance Engineering* **2005**, *26B*, 36−45.
(42) Lelli, M.; Chaudhari, S. R.; Gajan, D.; Casano, G.; Rossini, A. J.; Ouari, O.; Tordo, P.; Lesage, A.; Emsley, L. Solid-State Dynamic Nuclear Polarization at 9.4 and 18.8 T from 100 K to Room Temperature. *J. Am. Chem. Soc.* **2015**, *137*, 14558−14561.

https://doi.org/10.1021/acs.jpclett.3c00726
J. Phys. Chem. Lett. 2023, 14, 4748−4753